2021

An isotropic neo-hookean finite element model of healthy elastic arterial walls within commercial software

Ambrose, R.

The Plymouth Student Scientist
University of Plymouth

An isotropic neo-Hookean finite element model of healthy elastic arterial walls within commercial software

Reece Ambrose

Project Advisor: [Adam Kyte](), School of Engineering, Computing and Mathematics, University of Plymouth, Drake Circus, Plymouth, PL4 8AA

Abstract

A non-linear isotropic finite element model of an elastic arterial wall is developed within the ANSYS commercial software package. While progressively increasing complexity of the model, it is validated with analytical theory. Geometric nonlinearity is investigated and an iterative convergence method for the calculation of a solution-dependent axial force, which increases with artery deformation, is presented.

Neo-Hookean hyperelastic material models are fitted to existing uniaxial, biaxial, and shear experimental data from literature for both rubber and polyurethane elastomer to introduce material nonlinearity into the arterial wall model. A mesh independence study was performed to determine a suitable mesh and the elastomer materials were simulated, with the resulting pressure-diameter responses compared to a real artery.

Finally, the arterial wall model was fitted to existing experimental results for a rat carotid artery and a human subclavian artery, and the mechanical responses were compared. It was found that the model simulated the behaviour of the rat carotid artery well for up to 15% diametral strain with a root-mean-square error (RMSE) of 0.43 mm Hg. For the human subclavian artery model, the behaviour did not match well, with the pressure-diameter response diverging from the real artery after 2% diametral strain. However, it had a RMSE of 0.94 mm Hg below 2% diametral strain. Recommendations for further investigation are made to improve the model.

Keywords: Arterial walls, artery, carotid artery, elastomer, finite element analysis, geometric nonlinearity, hyperelastic, isotropic, large deflection, material model, neo-Hookean, non-linear, solution-dependent axial force, subclavian artery, validation

Introduction

Arterial walls are predominately made up of the materials elastin, collagen, and smooth muscle. The mechanical structure and properties of these materials determines an artery's mechanical behaviour. There is significant interest in the properties and behaviours of arteries, due the benefits this knowledge can bring for surgical procedures (Sommer *et al.*, 2018).

Elastic arteries play an important role in the circulatory system by storing elastic energy during cardiac systole, which is when the heart contracts and ejects blood into the elastic arteries. During cardiac diastole, which is when the heart's ventricles relax, elastic arteries recoil and release the stored energy and keeps the blood flowing (Patton & Thibodeau, 2010; Tortora & Derrickson, 2009). Because the heart pumps in cycles, flow is pulsatile in the arterial system (Boron & Boulpaep, 2017). The compliance of arteries allows the blood pressure to remain relatively constant despite the pulsatile flow and reduces the pressure pulsations to almost zero by the time the blood reaches the capillaries (Hall, 2015).

Models of arterial walls have become much more complex as arterial mechanics has developed and easily go beyond what is possible within commercial software and typically involve non-standard finite element codes (Kalita & Schaefer, 2008). Finite Element Analysis (FEA) is a method to numerically solve the structural governing equations by discretising the model as finite elements in a matrix (Hearn, 1997a). These elements make up a mesh of the model. This paper is focused on modelling a section of arterial wall within the ANSYS 2020 R2 student commercial software.

Aim

The aim is to develop a model of an elastic arterial wall within a commercial finite element code, simulate the mechanical response with different internal pressures, and compare results with those from experiments in relevant literature.

Objectives

1. Conduct a literature review to understand the material structure and mechanical properties and behaviours of arterial walls, the material mechanics of cylinders, and to review existing studies and models of arterial walls.
2. Starting with basic assumptions like a thin-walled cylinder, develop a finite element model of a section of artery within a commercial finite element code and progressively add complexity.
3. Conduct appropriate validation cases to ensure the relevant mechanics is simulated correctly.
4. Simulate mechanical behaviour when subjected to similar loads as those in experiments in literature and compare results.

Literature Review
This section gives an overview of the relevant literature that one needs to be aware of to understand the research.

Material Structure of an Elastic Artery
There are generally two types of arteries: elastic and muscular (Holzapfel, Gasser & Ogden, 2000). Arteries consist of 3 layers: the tunica intima, the tunica media, and the tunica externa.

Tunica intima
The tunica intima is the inner layer of an artery and consists of three components: the endothelium, the basement membrane, and the internal elastic lamina. Tortora & Derrickson (2009) state that the endothelium is a thin layer of flattened endothelial cells that lines the lumen of the cardiovascular system. Marieb & Hoehn (2015) describe the lumen as the 'blood-containing space' of a blood vessel. The endothelium is supported by a basement membrane, which consists of a framework of collagen fibres (Tortora & Derrickson, 2009). Other literature, like Marieb & Hoehn (2015), refer to this layer as the subendothelial layer. Tortora & Derrickson (2009) continues to explain that an internal elastic lamina forms the boundary with the tunica media, which is a thin layer of elastic fibres with openings, allowing diffusion between the intima and media.

Burton (1954) suggests that the contribution of the endothelial lining to the mechanical properties of arteries can be ignored. Holzapfel, Gasser & Ogden (2000) suggest that the entire intima layer's contribution to the mechanical properties of arteries is insignificant in healthy young people, due to being very thin. However, Holzapfel *et al.* warns that the intima's mechanical properties can become significant with age due to arteriosclerosis. Arteriosclerosis is a type of vascular disease that thickens and hardens the arterial wall, causing a reduction in the lumen size (Patton & Thibodeau, 2010).

Tunica media
The tunica media is the middle and thickest layer of an artery. It is comprised of smooth muscle, elastin and collagen fibrils, and an external elastic lamina (Holzapfel, Gasser & Ogden, 2000; Marieb & Hoehn, 2015). The tunica media layer varies the most across the different vessel types (Tortora & Derrickson, 2009).

For elastic arteries, the elastic fibres in the media are responsible for the recoil of the vessel after distention, Patton & Thibodeau (2010) explain. The smooth muscle controls the diameter of vessels through vasoconstriction or vasodilation (decrease or increase in lumen diameter respectively) but is relatively inactive in elastic arteries (Marieb & Hoehn, 2015). Tortora & Derrickson (2009) state that the internal and external elastic laminae are well-defined for this type of vessel. Sheets of elastin are concentrically layered with smooth muscle in elastic arteries (Marieb & Hoehn, 2015). Tortora & Derrickson (2009) refer to these sheets of elastin as the elastic lamella. Due to their similarity, the internal and external elastic laminae are 'hardly distinguishable' from the elastic lamella (Holzapfel, Gasser & Ogden, 2000).

Tunica externa
The tunica externa (also called the tunica adventitia) is the outer layer of a blood vessel. Marieb & Hoehn (2015) explain that it's mostly composed of loosely woven collagen fibres. In larger vessels, the tunica externa has its own blood vessels called the vasa vasorum, which means vessels to the vessels (Tortora & Derrickson, 2009). Nerve fibres and lymphatic vessels are also present. Patton & Thibodeau (2010) state that collagen fibres extend outwards from the tunica externa and connect to nearby structures, which anchors the blood vessel and keeps it open.

Mechanical Behaviours
As discussed in the previous section, there are three main materials that make up an elastic artery's tunica media and externa layers: elastic fibres, smooth muscle, and collagen fibres. Due to the amount and structure of these materials, arteries have complex mechanical behaviours.

The elastic behaviour of an artery is due to its elastic fibres. Patton & Thibodeau (2010) explain that elastic fibres are composed of elastin, which is a protein polymer, and form a highly elastic network that can achieve 100% strains. Holzapfel, Gasser & Stadler (2002) suggest that the smooth muscle cells in the tunica media are responsible for the viscoelastic behaviour of arteries. They also state that viscoelastic behaviour is less pronounced in larger arteries. As previously discussed, the smooth muscle in elastic arteries is relatively inactive. In conclusion, elastic arteries have a mostly passive mechanical behaviour and due to its relatively large size, it has a less pronounced viscoelastic behaviour.

Arteries have a non-linear behaviour due to its wavy collagen fibrils (Holzapfel, Gasser & Ogden, 2000). Collagen fibres are woven together to strengthen the arterial wall and keep the lumen open (Patton & Thibodeau, 2010). They do not strain above 2 or 3 percent. Although they are stiff in extension, they are also flexible (Patton & Thibodeau, 2010). When not under load, the collagen fibres are slack and wavy and thus do not contribute much to an artery's stiffness, Holzapfel, Gasser & Ogden (2000) explain. When the artery is loaded, collagen fibres are straightened, which increases the vessel's stiffness as more fibres are progressively recruited, protecting the vessel from rupturing (Holzapfel, Gasser & Ogden, 2000). As a result, the arterial stiffness is dominated by the elastic fibres at small loads, whereas it's dominated by collagen fibres at larger loads (Mozafari, Zhou & Gu, 2019). Burton (1954) suggests that the elastic fibres are responsible for producing maintenance tension against physiological blood pressures whereas the collagenous fibres have a protective supporting role.

Patel & Fry (1969) show that the arterial wall can be considered as cylindrically orthotopic. Holzapfel, Gasser & Stadler (2002) have stated that this assumption has been generally accepted and used by literature.

The arterial wall is pretty much incompressible within physiological loads and deformations (Holzapfel, Gasser & Ogden, 2000; Kalita & Schaefer, 2008). Kalita & Schaefer refer to the findings of Chuong & Fung (1984), which shows a maximum wall volume change of 1.26% when under a radial compression of 10 kPa (75 mmHg). The deformation of an incompressible material is isochoric, which means that there are no volume changes (Holzapfel & Gasser, 2007). Gasser, Ogden &

Holzapfel (2006) state that, although an artery is classified as a mixture composite, it can be regarded as a homogenised solid for most studies of stress distribution.

Kyriakides & Yu-Chung (1991) explains that an elastic cylindrical tube experiences instability under large deformation and develops a local bulge that propagates axially. Burton (1954) analytically showed that there is a specific pressure at which a cylindrical vessel would experience a blow-out where the volume distensibility becomes infinite.

Material Mechanics of Cylinders
When a cylinder is subjected to internal pressure, three perpendicular principle stresses are set up in the wall, which are called the hoop, radial, and longitudinal stresses (Hearn, 1997b). Roark (2000) explains that if the cylinder walls are relatively thin, then the hoop and longitudinal stresses are practically uniform across the thickness of the wall and the radial stress and any bending stresses are negligible. Hearn (1997b) explains that the wall thickness should be less than 1/20th the diameter to be considered thin. He derives the following equations for hoop and longitudinal stresses. The longitudinal stress equation applies if there are end plates.

$$\sigma_H = \frac{pd}{2t} \qquad (1) \qquad\qquad \sigma_L = \frac{pd}{4t} \qquad (2)$$

For cylinders with a wall thickness greater than 1/20th the diameter, the hoop and longitudinal stresses are not uniform across the wall and the radial stress is no longer negligible (Roark, 2000). Hearn (1997b) gives the equations below for a thick-walled cylinder.

$$\sigma_H = A + \frac{B}{r^2} \qquad (3) \qquad\qquad \sigma_r = A - \frac{B}{r^2} \qquad (4)$$

$$\sigma_H = p \left[\frac{\left(\frac{R_2}{r}\right)^2 + 1}{k^2 - 1} \right] \qquad (5) \qquad\qquad \sigma_r = -p \left[\frac{\left(\frac{R_2}{r}\right)^2 - 1}{k^2 - 1} \right] \qquad (6)$$

$$\sigma_L = \frac{p_1 R_1^2 - p_2 R_2^2}{R_2^2 - R_1^2} \qquad (7) \qquad\qquad \varepsilon_H = \frac{1}{E}(\sigma_H - v\sigma_r - v\sigma_L) \qquad (8)$$

$Where\ k\ is\ the\ diameter\ ratio$
$$D_2/D_1 = R_2/R_1$$

Equations (3-4) are the Lamé equations for thick-walled cylinders, where constants A and B are to be determined from boundary conditions (Hearn, 1997b). Equations (5-6) are the hoop and radial stresses when the cylinder is subject to internal pressure only. Hearn (1997b) derived these from equations (3-4) with the following boundary conditions: at $r = R_1$, $\sigma_r = -p$ and at $r = R_2$, $\sigma_r = 0$ (Hearn, 1997b). Equation (7) is the longitudinal stress when there are end plates, which can be used for the cases of internal pressure only or both internal and external pressures. Equation (8) is the strain formula.

Hearn (1997b) describes an isotropic material as one that 'exhibits uniform properties throughout in all directions' with the opposite being anisotropic. Orthotropic materials have different properties in different planes (Hearn, 1997b). For a cylindrically orthotropic material, there are three independent elastic moduli in the circumferential, longitudinal, and radial directions, Patel & Fry (1969) explain.

Hearn (1997b) explains that when a simple bar is loaded longitudinally and within the elastic range, lateral strains are induced. This is represented in equation (9) by Poisson's ratio of lateral strain to longitudinal strain (Hearn, 1997b):

$$\nu = \frac{-\delta d/d}{\delta L/L} \qquad (9)$$

Elastomeric Materials and Hyperelastic Modelling
Elastomers have a strongly non-linear stress-strain relation known as hyperelasticity and exhibit large strains (Sasso *et al.*, 2008). Sasso *et al.* explain that hyperelastic material behaviour can be characterised by constitutive models, which can be fitted to experimental data to determine material parameters. Ogden explains that "an elastic material for which a strain-energy function exists is called a Green elastic or hyperelastic material' (Ogden, 1984, p.206). Hyperelastic models are defined by this strain-energy function, which measures the amount of energy stored in the material due to deformation (Sasso *et al.*, 2008).

Marckmann & Verron (2006) evaluated and compared the ability of hyperelastic models to reproduce behaviours of elastomers. With a single material parameter, the neo-Hookean constitutive equation is the simplest physically-founded model and they suggest that it should be used for strains below 150%. Marckmann & Verron explain that it's derived from molecular chain statistics considerations.

ANSYS Workbench provides hyperelastic material models which are isotropic and constant with respect to temperature and are assumed to be nearly or purely incompressible. Its neo-Hookean model is one of them:

$$W = \frac{\mu}{2}(\overline{I_1} - 3) + \frac{1}{d}(J - 1)^2 \qquad \text{(ANSYS Inc, 2011)} \quad (10)$$

Where:
W = strain energy per unit reference volume
$\overline{I_1}$ = first deviatoric strain invariant
μ = initial shear modulus of the material
d = material incompressibility parameter
J = determinant of the elastic deformation gradient F

There are papers that propose custom models, but the implementation of these would require coding custom material models into ANSYS Mechanical APDL, which is outside the scope of this paper. Examples of constitutive models are Holzapfel,

Gasser & Ogden (2000), Demiray & Vito (1991), and von Maltzahn, Besdo & Wiemer (1981).

For the investigation of hyperelasticity in this paper, two elastomers are considered. Treloar (1944) performed experiments on vulcanised rubber. The uniaxial and biaxial extension and shear test data has been compiled by Anssari-Benam & Bucchi (2021), who used the data to test how well their proposed neo-Hookean strain energy function modelled large deformations of incompressible elastomeric materials. Kanyanta & Ivankovic (2010) investigated the behaviour of polyurethane elastomer with variations in temperature, humidity, and strain rate and performed mechanical tests. The test data for both the rubber and polyurethane elastomer are illustrated in Figure 1.
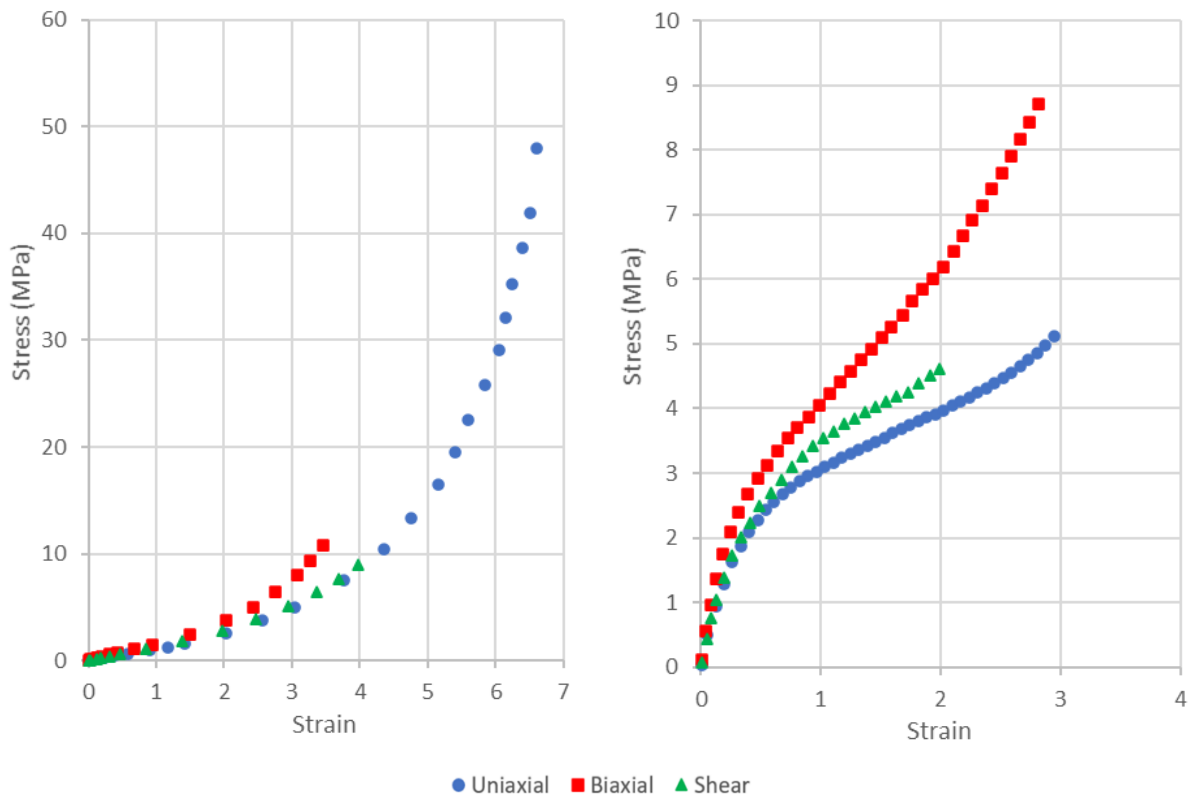
Figure 1: Experimental data for Treloar's rubber (left) and Kanyanta & Ivankovic's polyurethane (right)

Artery Experimental Data

Weizsacker & Pinto (1988) studied the passive biomechanical response of rat carotid arteries and compared it to rubber tubes and investigated the isotropy and anisotropy of the arterial wall. They show that the elasticity of arteries is similar to that of rubber tubes. During the experiment, the rubber tube experienced an aneurysm.

Sommer *et al.* (2018) investigated the differences in biomechanical properties between similar sized subclavian and iliac arteries. Arteries were subjected to axial strains, transmural pressures, and torsion through extension-inflation-torsion experiments. Axial and circumferential residual stresses were determined, and the

microstructure was investigated. Kamenskiy *et al.* (2014) also experimented on subclavian arteries.

Thin and Thick-Walled Cylinders

This section details the development of a simple cylinder model of arterial wall while simultaneously completing validation cases. These validation cases show that the model results agree with those from analytical calculations. For each progressive version of the model, it is important to understand the material mechanics involved and to check that the model was set up correctly. Stresses and strains were obtained from the model at points across the cylinder wall and statistically compared to analytical calculations. Different loading and boundary conditions are considered in different validation cases to better understand how the model setup affects results.

Investigation

(a)   (b)
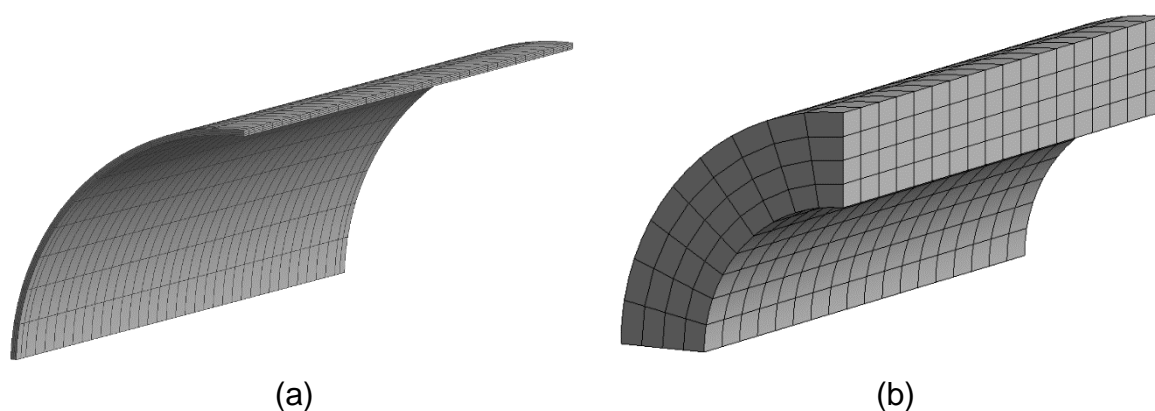
**Figure 2:** Meshes of the (a) thin-walled cylinder and (b) thick-walled cylinder

Using static-structural analysis in ANSYS, simple quarter-cylinders were modelled, as shown in Figure 2. The use of quarter-cylinders reduces mesh size and hence solve time while behaving like full tubes. The thin and thick-walled cylinders have the same length and outside radius but have a different wall thickness. Dimensions are summarised in Table 1.

Table 1: Cylinder Dimensions

Dimension (mm)	Thin Model	Thick Model
Inner Radius	3.9	2.5
Outer Radius	4.0	4.0
Wall Thickness	0.1	1.5
Length	10.0	10.0

Structural steel is used for the material and an internal pressure of 1 MPa is applied. For the thick-walled cylinder, inside and outside radii were set to 2.5 and 4 mm, which is similar to the subclavian arteries from Sommer *et al.* (2018). Model parameters like dimensions, internal pressure, and material properties are arbitrary for these cases because the aim of them is to validate the model.

The ANSYS default global mesh size was used, and edge sizing controls were applied to the wall thickness to set the number of divisions across the wall to 4. Only a simple mesh is needed at this stage; a mesh independence study is later performed. To model a full cylinder as a quarter-cylinder, frictionless constraints are applied to the cut faces. One end face is constrained from moving in the axial direction while the other is free to move. Results are taken halfway along the cylinder from the inner radius to the outer radius, as shown by the illustrated path in Figure 3.
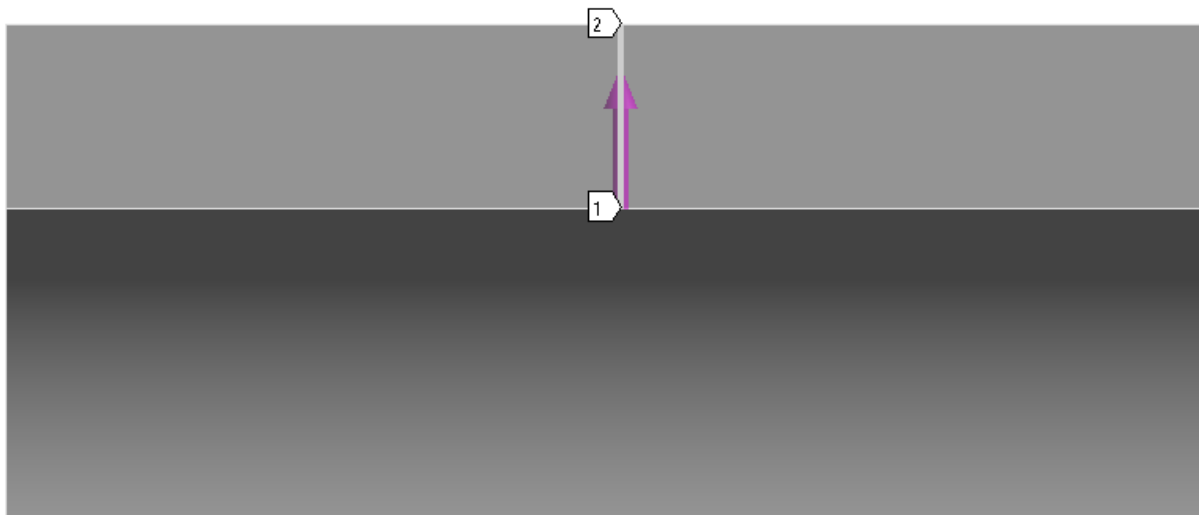
Figure 3: Radial position path along wall thickness

The following cases are investigated:
- Thin-walled cylinder
- Thick-walled cylinder
- Thick-walled cylinder constrained from axial deformation
- Thick-walled cylinder with end plates
- Thick-walled cylinder subject to both internal and external pressure and with end plates

The thin-walled cylinder validation case was used to quantify the amount that the inner and outer stresses differ from thin-walled cylinder theory. The thick-walled cylinder validation cases demonstrate how end plates, a zero axial deformation boundary condition, and the addition of external pressure affects cylinder stresses and strains.

For analytically validating the axial stress for a thick-walled cylinder constrained from axial deformation, equation (11) was used, which was derived from equation (8).

$$\sigma_L = \nu(\sigma_r + \sigma_H) \tag{11}$$

When considering end plates, they are simulated by applying an axial force to the free end face of the model. This cylinder axial force can be determined by multiplying the internal pressure by the inner cylinder cross-sectional area, as shown by equation (12). The use of an axial force removes the requirement to physically model end plate geometry. Equation (13) determines the force used for the model because

it is a quarter-section of a cylinder and thus, the force must be divided by four. For the thick-walled cylinder, the model axial force is calculated to be 4.91 N.

$$F = p\pi R_1^2 \qquad (12) \qquad\qquad F = \frac{p\pi R_1^2}{4} \qquad (13)$$

When considering external pressure, equations (14-15) give the analytical hoop and radial stresses. These have been derived from the Lamé equations using the boundary conditions $r = R_1$, $\sigma_r = -p_1$ and at $r = R_2$, $\sigma_r = p_2$. Analytical axial stress was calculated using equation (7). An external pressure of 0.1 MPa was applied.

$$\sigma_H = \frac{p_1 - p_2 k^2 + \frac{R_2^2}{r}(p_1 - p_2)}{k^2 - 1} \qquad (14)$$

$$\sigma_r = \frac{p_1 - p_2 k^2 - \frac{R_2^2}{r}(p_1 - p_2)}{k^2 - 1} \qquad (15)$$

Results and Discussion

Tables 2 and 3 show the model and analytical results for the thin-walled cylinder. Radial stresses are ignored as they can be neglected for thin-walled cylinders (Hearn, 1997b). The model hoop stress decreases from 39.64 to 38.64 MPa from the inner to outer radii. This shows a negligible difference as the hoop stress at the inner radius is only 2.59% greater than at the outer radius. This is expected because the wall thickness to inner diameter ratio is 1/78, which is much less than the 1/20 specified by Hearn (1997b) for the thin-walled assumption. The model axial stress is so small that it is considered zero, as expected.

**Table 2:** Thin-walled assumption cylinder analytical results

Wall Thickness (mm)	Hoop Stress (MPa)	Axial Stress (MPa)	Hoop Strain	Axial Strain
0.1	39.00	0.00	1.95E-04	-5.85E-05
1.5	1.67	0.00	8.33E-06	-2.50E-06

Table 3: Model results for the thin-walled cylinder

Radial Position (mm)	Hoop Stress (MPa)	Axial Stress (MPa)	Hoop Strain	Axial Strain
3.900	39.64	-1.06E-06	2.00E-04	-5.78E-05
3.925	39.38	2.75E-08	1.98E-04	-5.78E-05
3.950	39.13	3.82E-08	1.97E-04	-5.78E-05
3.975	38.88	1.29E-06	1.95E-04	-5.78E-05
4.000	38.64	1.44E-06	1.93E-04	-5.78E-05

Model results for the thick-walled cylinder cases are shown in Figure 4 for stresses and Figure 5 for strains. The hoop and radial stresses and strains significantly change from the inner to outer surfaces. This cylinder has a wall thickness to inside

diameter ratio of 3/10, which is much larger than the 1/20 recommended for the thin-walled assumption. A constant axial strain is induced due to the hoop and radial stresses because of the Poisson effect.
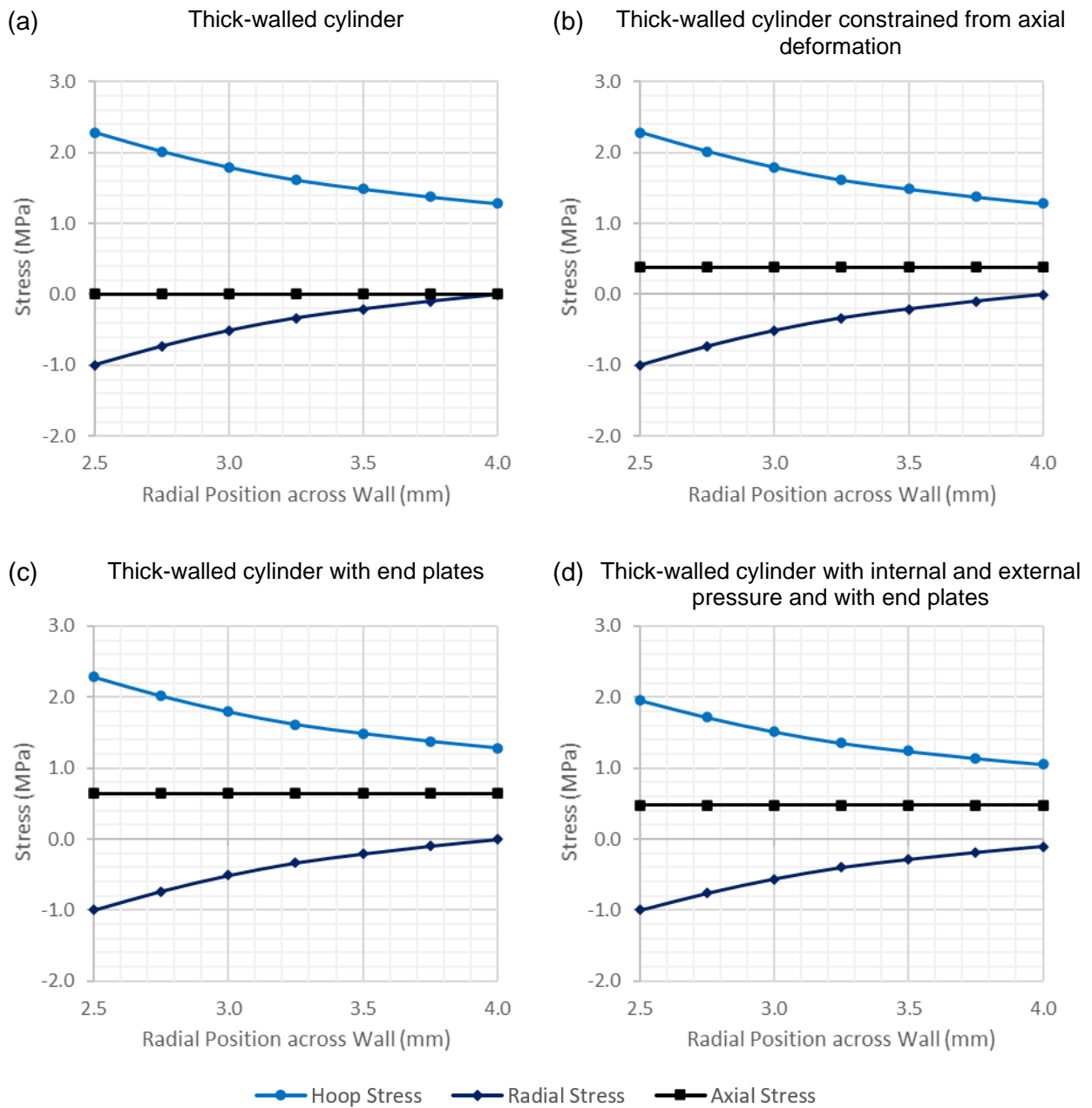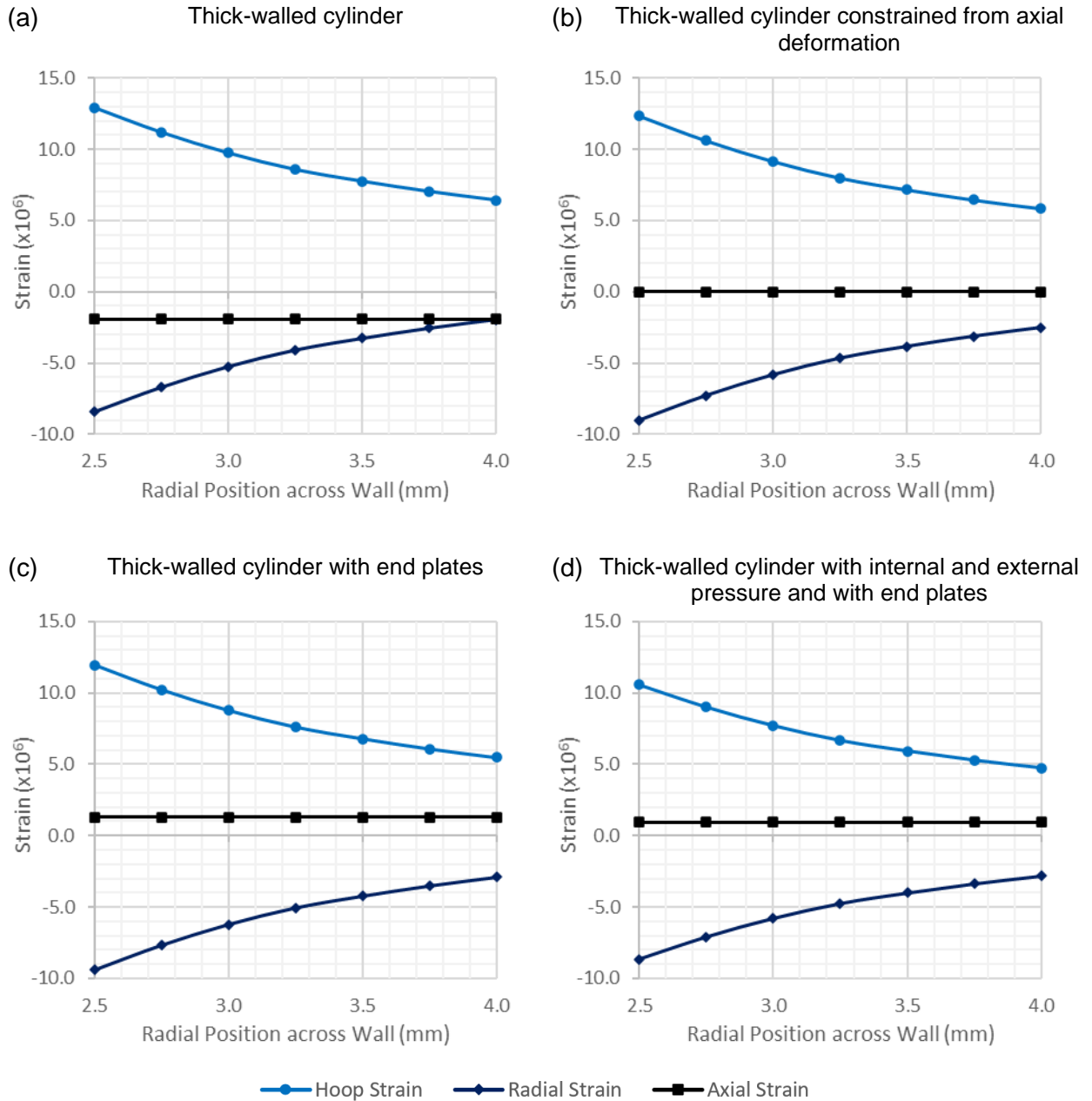

Figure 4: Stresses across wall for the thick-walled cylinder validation cases

As shown by graphs (b), if the cylinder is constrained from deforming axially then axial stresses are induced. This is because axials strains are still laterally induced by the hoop and radial stresses but, because of the zero axial strain constraint, axial stresses are produced to cancel them out. Hoop and radial stresses are unaffected; however, hoop and radial strains have slightly changed due to the axial stress inducing lateral strains in the hoop and radial directions.

For the thick-walled cylinder with end plates, the applied axial force produces a constant axial stress and strain along the wall thickness and this in turn induces lateral strains that affect the hoop and radial strains. Hoop and radial stresses are unchanged from the (a) thick-walled cylinder case.

Figure 4(d) shows that an external pressure reduces the hoop and axial stresses for a thick-walled cylinder with end plates. The radial stresses at the inner and outer radii are equal in magnitude to the internal and external pressures respectively, but they are negative because the pressures radially compress the cylinder wall.

Figure 5: Strains across wall for the thick-walled cylinder validation cases

Table 4 presents the root-mean-square errors (RMSE) for the stresses and strains which shows how well the model and analytical results match. The RMSEs are very

small relative to the values in figures 4 and 5, which shows that the model and analytical calculations strongly agree. In conclusion, these validation cases have scoped out loading and boundary conditions and demonstrated that the model complies with analytical theory.

Table 4: RMSE of the model and analytical results for the thick-walled cylinder validation cases

	Thick-Walled Cylinder Validation Case			
	(a)	(b)	(c)	(d)
Hoop Stress RMSE (MPa)	0.010	0.010	0.010	0.009
Radial Stress RMSE (MPa)	0.010	0.010	0.010	0.009
Axial Stress RMSE (MPa)	0.000	0.000	0.000	0.000
Hoop Strain RMSE (x10^6 strain)	0.067	0.067	0.067	0.060
Radial Strain RMSE (x10^6 strain)	0.067	0.067	0.067	0.060
Axial Strain RMSE (x10^6 strain)	0.000	0.000	0.000	0.000

Geometric Nonlinearity
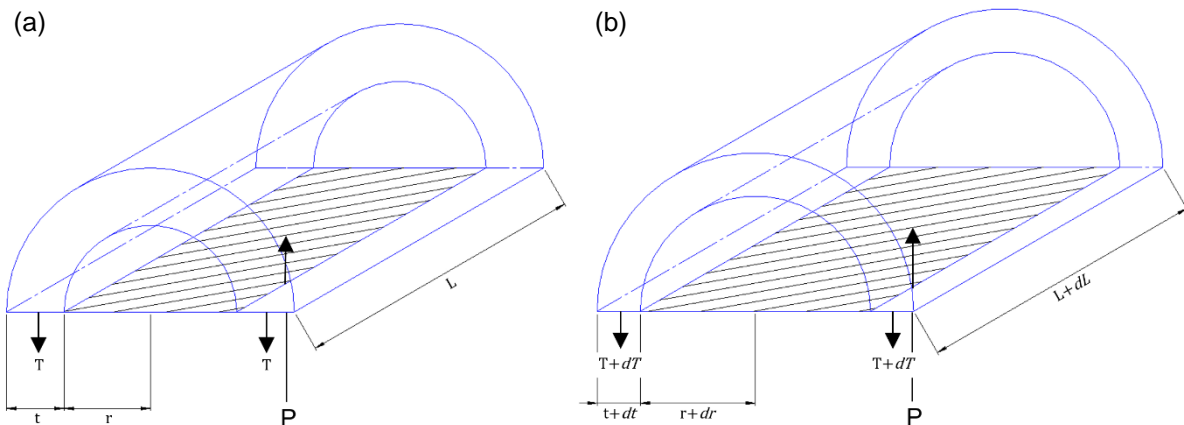
Figure 6: Large deflection of a cylinder under constant pressure with (a) showing the undeformed cylinder and (b) the deformed cylinder

When cylinder deformation is large, its geometry changes. This affects the behaviour of a real cylinder because the projected area upon which the internal pressure P is acting increases, as shown by Figure 6. With a constant pressure but increasing projected area, the resulting force increases. Therefore, the wall tension T must increase to maintain force equilibrium and thus the hoop stress increases. Also, the wall thickness decreases as the cylinder deforms due to the compressive radial stress which further increases hoop stress. The resulting behaviour is decreasing cylinder stiffness as deformation increases.

This large deformation behaviour can be captured within ANSYS simply by enabling the large deflection option in analysis settings. Both thin and thick-walled models with large deflection have been validated by checking that they are in force

equilibrium using the Lamé equations for hoop stress. While this method does not analytically calculate the final geometry or stresses, it uses the model's results to show it is in mechanical equilibrium.

Large Deflection Validation
For the thin-walled model, an internal pressure of 1.5 kPa is applied and the material was set to structural steel but with the Young's modulus modified to 0.5 MPa. This pressure and Young's modulus were chosen to ensure adequate deformation so that large deflection effects are non-negligible.

The average model hoop stress across the cylinder wall was 0.07086 MPa. Using the geometric dimensions of the loaded model, the analytical hoop stress was calculated to be 0.07058 MPa. The analytical value is close to the model's with a percentage error of 0.4%. This validates the thin-walled model because the model hoop stress matches the stress needed to keep the deformed geometry in force equilibrium.

For the thick-walled model, the same material is used but a larger pressure of 30 kPa is applied to ensure adequate deformation. The analytical hoop stress was calculated at both the inner and outer radii using the dimensions of the loaded model. Table 5 summarises the model and analytical hoop stresses. The analytical values are within 3.6% and 3.0% of the model values for the inner and outer radial locations respectively, which adequately shows that the model is in force equilibrium.

Table 5: Thick-walled cylinder large deflection validation

Radial Location	Model Hoop Stress (MPa)	Analytical Hoop Stress (MPa)
Inner	0.0853	0.0822
Outer	0.0507	0.0522

Solution-Dependent Axial Force
An applied axial force to a thick-walled cylinder is constant and does not change with the geometry. However, it should increase with the square of the inner radius as per equation (15). This axial force is the result of the internal pressure on imaginary end plates.

For a given internal pressure, there is a specific axial force that, when also applied, will stretch the cylinder so that the final inner radius corresponds to the applied axial force as per equation (15). An iterative convergence method is developed to solve this axial force by recalculating it until it converges:

$$F = \frac{p\pi r_i^2}{4} \tag{15}$$

$$\text{Axial Force Percentage Error} = \frac{F_{updated} - F}{F} \times 100\% \tag{16}$$

1. Calculate the axial force using equation (15) and the initial inner radius of the model.
2. Apply this axial force to the model and run.
3. Recalculate the axial force using the final inner radius from the model results. Consider the recalculated axial force $F_{updated}$ and the prior axial force F.
4. Calculate the axial force percentage error using equation (16).
5. If the axial force percentage error meets the convergence criterium, stop. Otherwise, apply the updated axial force to the model and rerun. Repeat steps 3 to 5.

A convergence criterium of less than 0.1% was chosen because it achieves excellent accuracy while only requiring two to three iterations for convergence. More iterations are needed for larger stetches because the initial error in axial force will be larger. This iterative convergence method produces a solution-dependent axial force (SDAF) for the given internal pressure, which removes the need for physically modelling end plates.

Results and Discussion

The geometric nonlinearity effects of the large deflection (LD) option and the solution-dependent axial force (SDAF) on model behaviour is shown in Figure 7. LD on captures geometric nonlinearity due to the internal pressure whereas applying the SDAF captures geometric nonlinearity due to the axial force. Diametral stretch is defined at the outer radius to show the amount of inflation of the whole cylinder. Axial stretch is constant across the cylinder wall and it shows the amount of lengthening or shortening.

The results show that the LD option produces a decreasing diametral stiffness whereas the SDAF produces a slight increasing diametral stiffness. SDAF produces positive axial stretch which lengthens the cylinder at an increasing rate. When combined, the cylinder expands and lengthens at an increasing rate with internal pressure, which means a decreasing cylinder stiffness. This would translate to an increasing volume distensibility as discussed by Burton (1954) and would cause a blow-out at a particular threshold pressure.

Due to convergence issues at larger strains, the model was only simulated for diametral strains below approximately 20%. Some investigation was done into these issues, but it was abandoned due to time constraints. The issues are likely due to time control settings, boundary conditions, and the need to refine the mesh as it deforms.
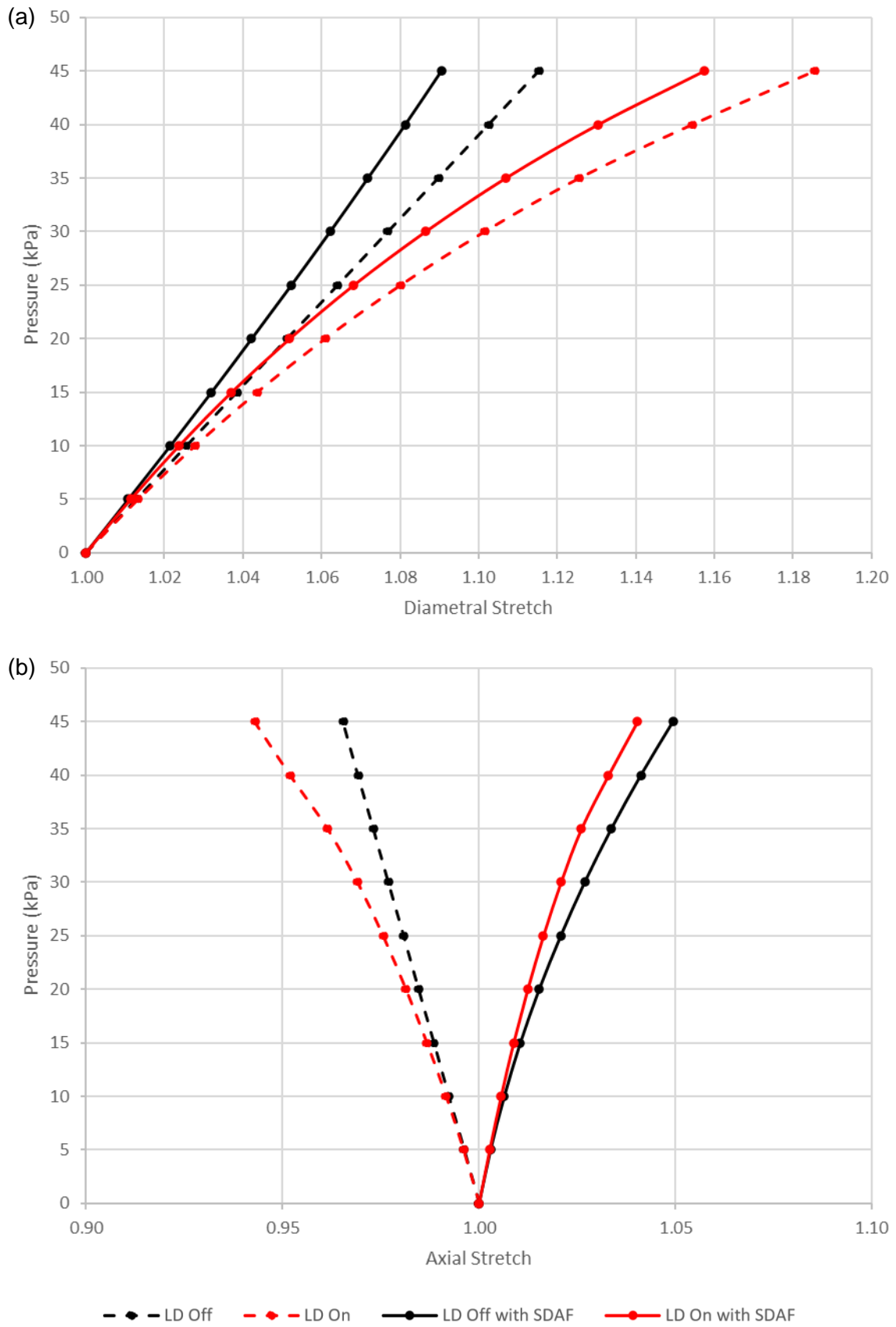
Figure 7: The effect of geometric nonlinearity on model behaviour with (a) showing diametral stretch and (b) axial stretch

Isotropic Hyperelastic Model

This section introduces material non-linearity into the artery model using hyperelastic material models. Rubber and polyurethane experimental data are used to curve fit Neo-Hookean models. These elastomer materials are used in the artery model to show how the mechanical response compares to that of Weizsacker & Pinto's (1988) rat carotid artery. Weizsacker & Pinto showed that an arterial segment behaves like rubber tubes. Lastly, the arterial wall model is curve fitted to the rat carotid artery (CA) and Sommer *et al.*'s (2018) human subclavian artery (SA).

Using the curve fitting functionality in ANSYS Engineering Data, a Neo-Hookean model was curve fitted to rubber experimental data produced by Treloar (1944). Figure 8 shows this data and the curve fits for up to a 200% strain. As discussed by Marckmann & Verron (2006), the Neo-Hookean model is suitable for strains below 150%. It has been chosen for the final model because the strains of interest are small and it involves only a single material parameter, which will make model fitting to artery experimental data simple. This process was repeated for the polyurethane experimental data produced by Kanyanta & Ivankovic (2010).
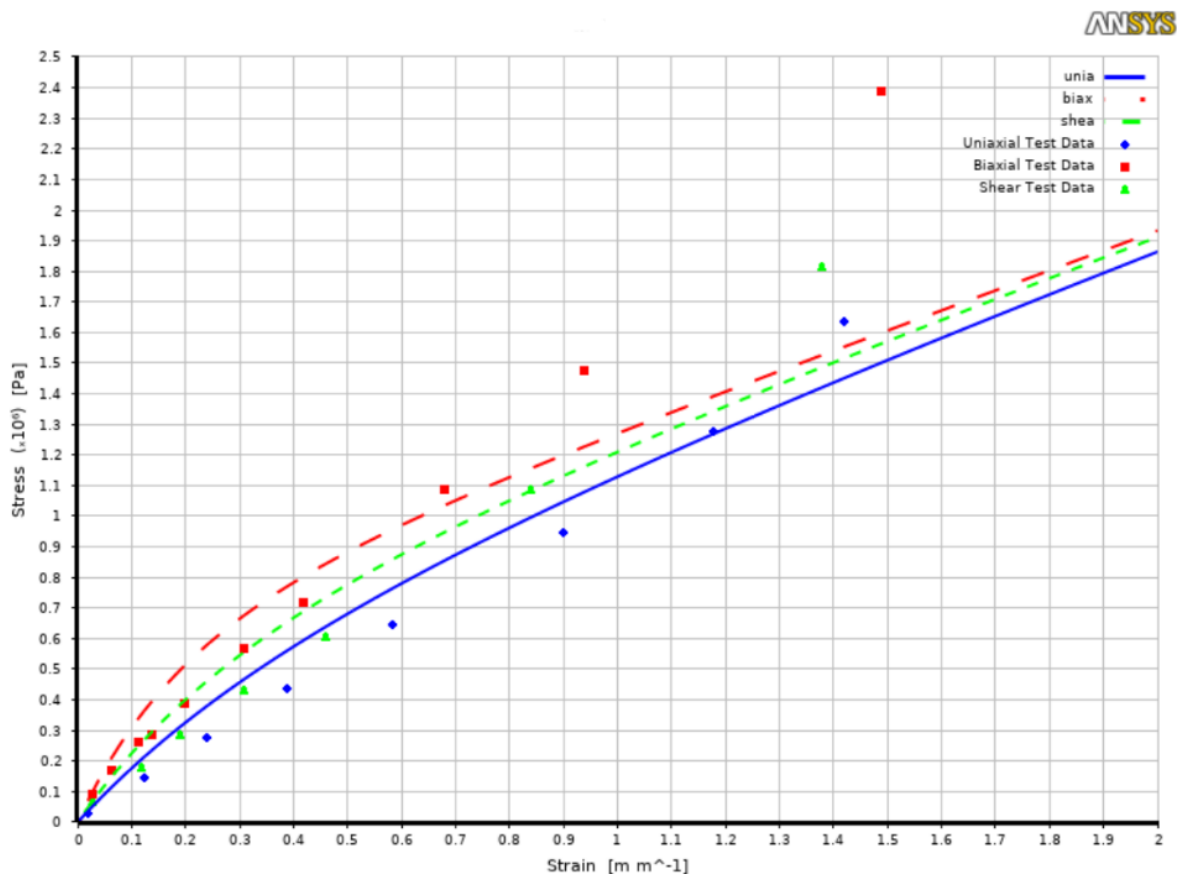

Figure 8: Neo-Hookean curve fit of Treloar's rubber experimental data (1944)

Mesh Independence Study

A mesh independence study was performed to determine a suitable mesh for the final arterial wall model. The Treloar rubber neo-Hookean material is used along with the geometry of the rat CA, which is an inner radius of 0.437 mm, an outer radius of

0.538 mm, and a chosen length of 1.5 mm. A suitable loading scenario needed to be chosen for this study. Therefore, a series of simulations were performed using the standard mesh sizings from earlier models (default global mesh with 4 radial divisions) to map out the pressures and strains.

The maximum pressure simulated was 600 mm Hg, which gave a hoop strain of 18.8%. The 400 mm Hg pressure and its corresponding SDAF value produced a 10.3% hoop strain. This was chosen as the loading scenario for the mesh independence study because it is in the middle of the considered hoop strain range. The results from the mesh independence study in Figure 9 show that the number of radial divisions has the greater impact on the resulting hoop strain and the solve time. The number of axial divisions had negligible effect.
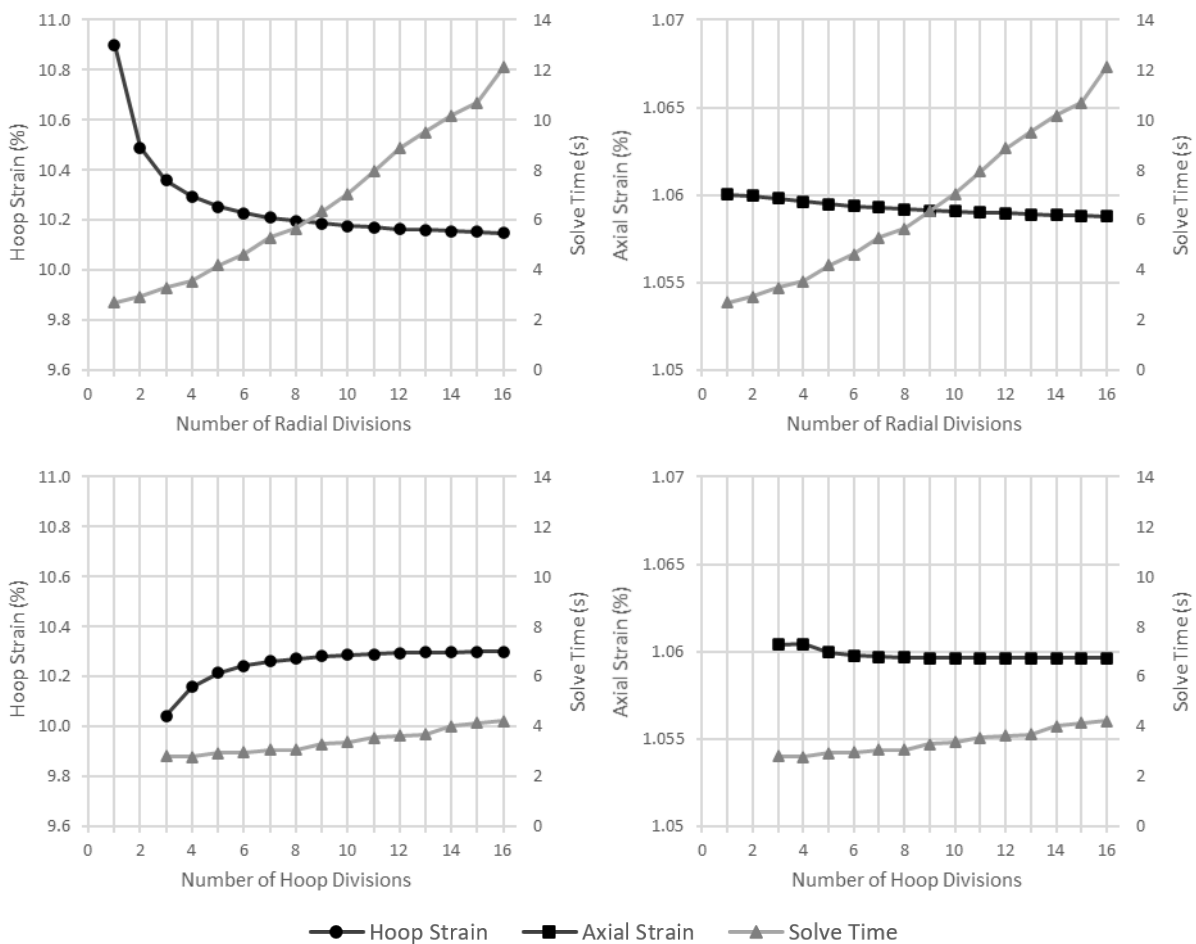
Figure 9: Mesh independence of radial and hoop divisions for model hoop and axial strains

As shown by Figure 10. The number of divisions for the final mesh was chosen to be 4, 20, and 40 for the radial, hoop, and axial directions, respectively. The radial divisions number was kept at 4 because increasing it would mean increasing the number of divisions in the other directions to maintain suitable element aspect ratios, which would result in a much larger number of elements. The percentage difference in hoop strains between 4 and 16 radial divisions is 1.5%, which was considered

acceptable. The number of hoop and axial divisions was chosen to ensure suitable element aspect ratios.
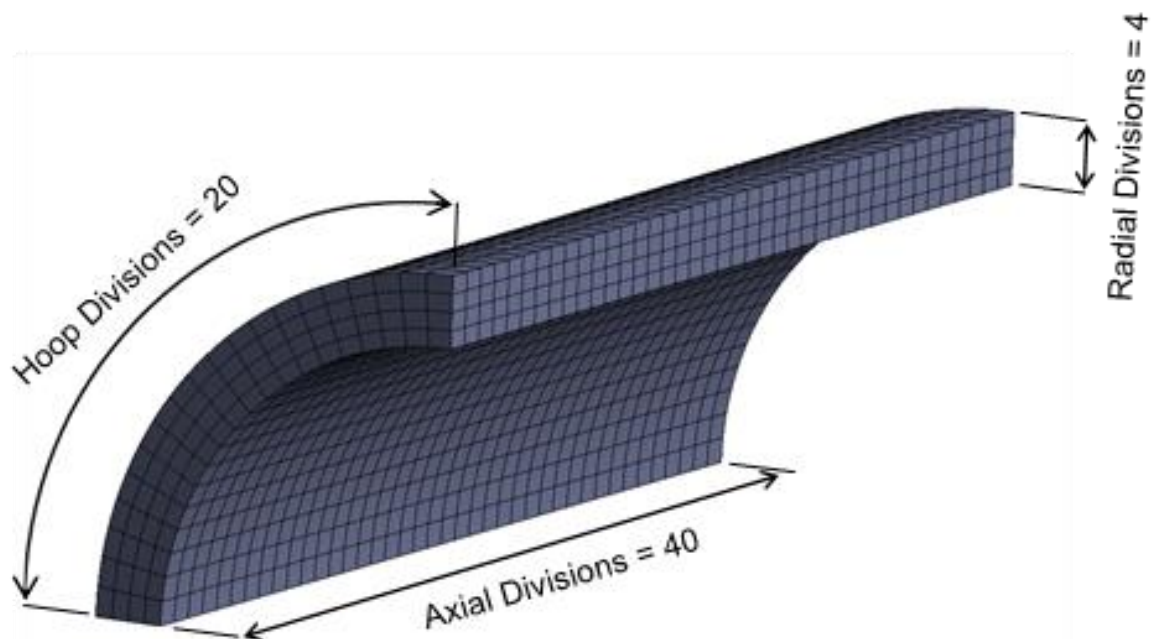

Figure 10: Final Mesh

Mechanical Responses of the Hyperelastic Artery Models

Using the curve fitted neo-Hookean material models for Treloar's (1944) rubber and Kanyanta & Ivankovic's (2010) polyurethane elastomer, the models' responses were simulated and are shown in Figure 12. To allow comparison with the rat CA, the loading and unloading paths from Weizsacker & Pinto's (1988) response were extracted and averaged to get the pressure-diameter response shown in Figure 11.

The elastomer artery models have much stiffer pressure-diameter responses than Weizsacker & Pinto's (1988) rat CA. Therefore, the model is curve fitted to experimental data from a real artery so that the behaviour can be better compared. This makes the artery model's pressure-diameter response start with the same gradient as the real artery. Curve fitting was done by adjusting the material parameter of the neo-Hookean material model. A gradient factor was determined by dividing the initial gradient of the rubber artery model response by the initial gradient of the real artery response. Then, the material parameter of the rubber neo-Hookean material model was multiplied by this factor.
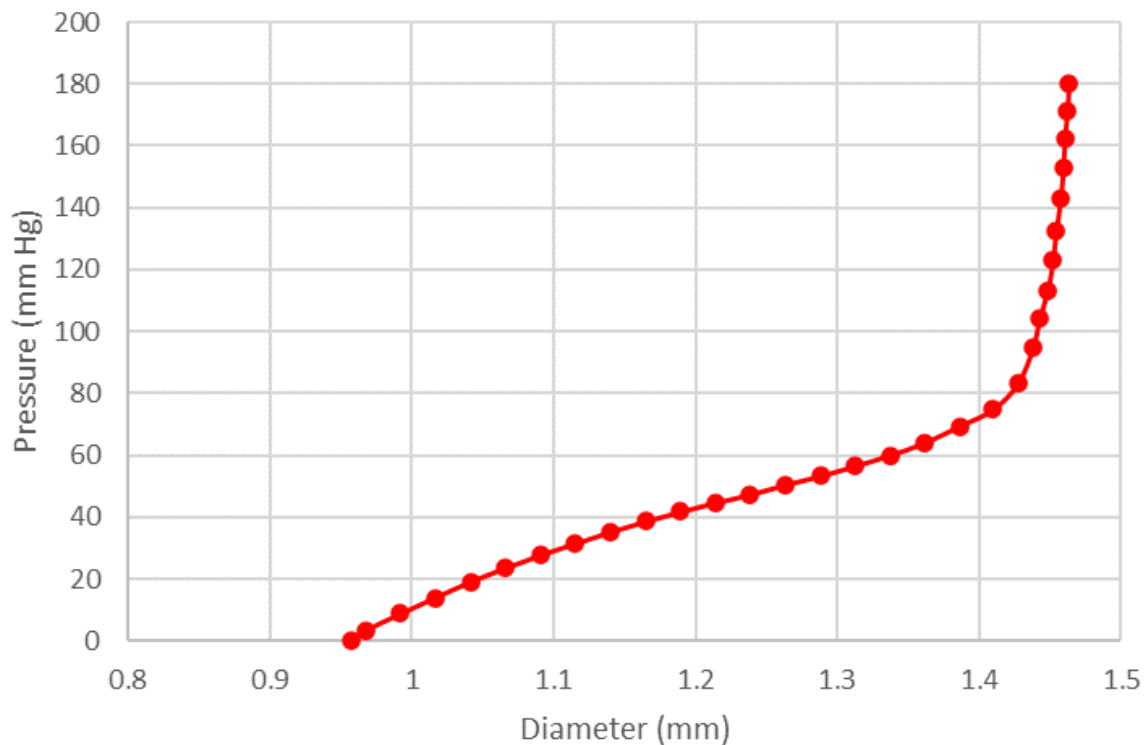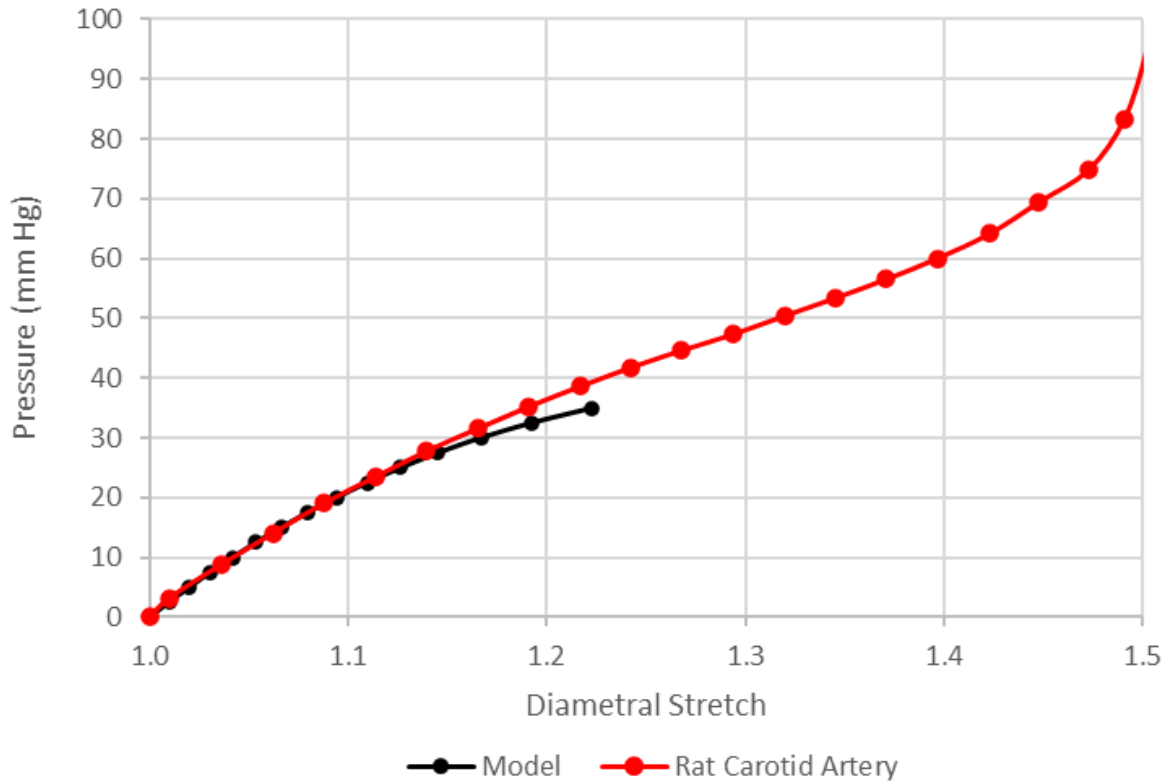
Figure 11: Averaged loading and unloading pressure-diameter response of Weizsacker & Pinto's (1988) rat carotid artery
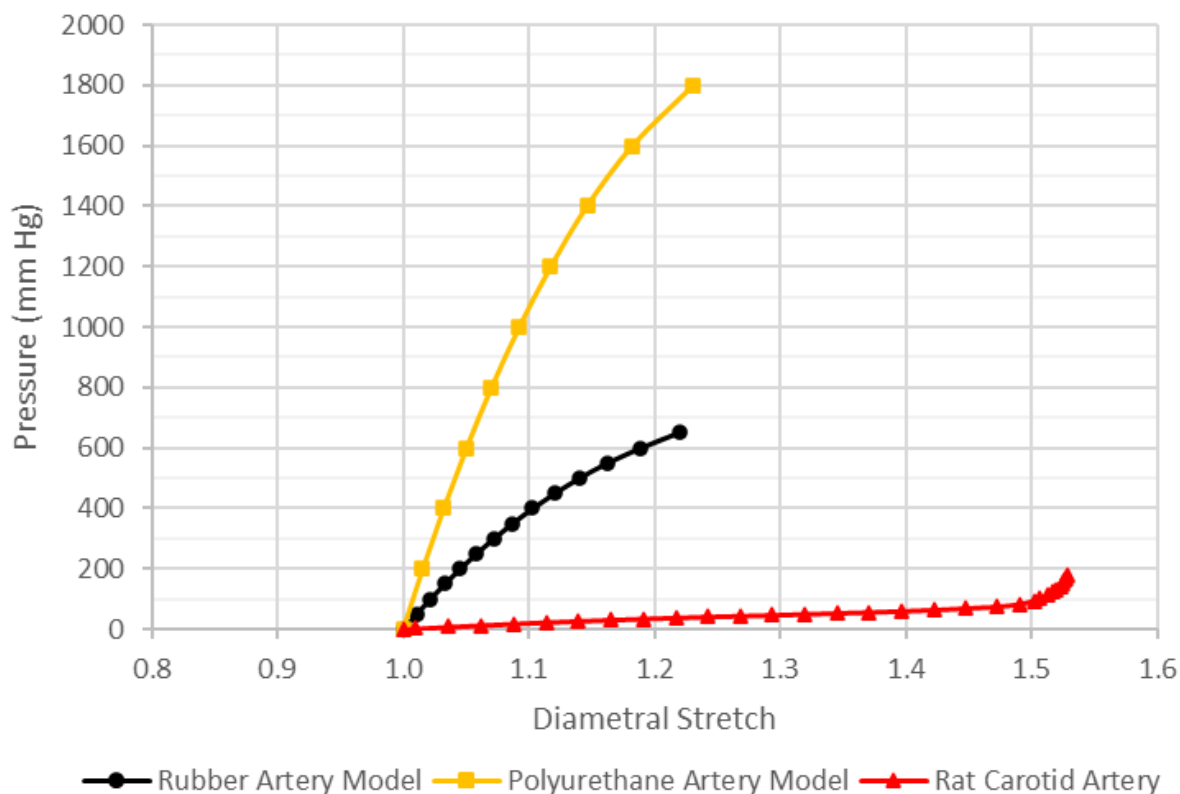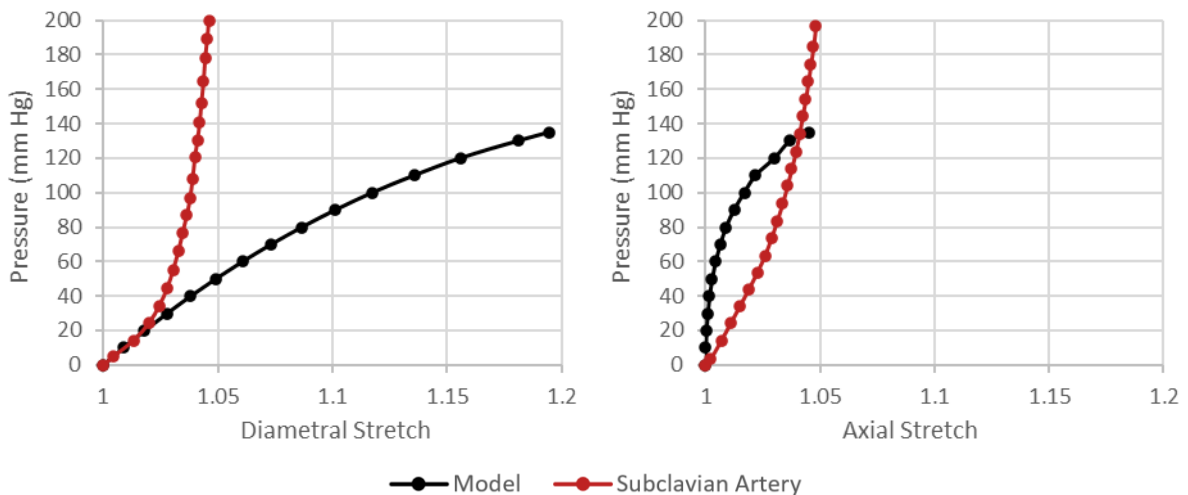

Figure 12: Pressure-diameter responses of the rubber and polyurethane artery models compared to Weizsacker & Pinto's (1988) rat carotid artery

Results and Discussion

The pressure-diameter responses of the fitted models for Weizsacker & Pinto's (1988) rat carotid artery (CA) and Sommer *et al.*'s (2018) human subclavian artery (SA) are shown in Figures 13 and 14.

Figure 13: Pressure-diameter responses of the model and Weizsacker & Pinto's (1988) rat carotid artery

Figure 14: Pressure-diameter (left) and pressure-axial (right) responses of the model and Sommer *et al.*'s (2018) subclavian artery

The pressure-axial response is shown for the SA. The illustrated rat CA response is the same as in figure 11 and is the averaged loading and unloading path of Weizsacker & Pinto's experimental data. This is because hysteresis was not of interest in this paper and Weizsacker & Pinto observed that the hysteresis loop is quite slim.

The CA model was simulated up to approximately 23%, which is where convergence issues prevented solving as discussed earlier. After approximately 15% diametral strain, the model starts to diverge from the rat CA. For the entire simulated range, there is a RMSE of 1.47 mm Hg. However, when considering strains of below 15%, which is where the model's response matches the artery, a RMSE of 0.43 mm Hg is calculated. This shows that the model simulates the behaviour of the rat CA well for up to 15% diametral strain. The RMSE could be further improved by giving the model a larger initial gradient, however, it was kept the same so that the responses can be compared easily.

For the SA model, the dimensions of Sommer *et al.*'s (2018) patient II were used along with a length of 9.2 mm. The mesh settings are the same as those used for the rat CA and this length was chosen to maintain the same length to outer radius ratio. Figure 14 shows that the model simulates the pressure-diameter response of the SA well up to 2% diametral strain, where it then diverges significantly as the real artery stiffens. The RMSE for up to 2% diametral strain is 0.94 mm Hg.

When considering the axial response, the model behaves differently to the real artery. The axial response has a decreasing gradient throughout the range whereas the real artery has an increasing gradient. The initial gradients likely differ due to the isotropic assumption. Arterial walls can be considered cylindrically orthotropic and so the stiffness differs in the axial and circumferential directions (Patel & Fry, 1969). Sommer *et al.* (2018) experimented with various axial pre-stretches and the results showed that increasing the axial pre-stretch for the SA led to a softer response. Therefore, the model may fit to a SA with a larger pre-stretch better. Axial pre-stretch was not considered in the model's development and the SA had an axial pre-stretch of 1.0 whereas the rat CA's was 1.74.

The human SA is much stiffer than the rat CA. The decreasing gradient for the CA's pressure-diameter response allows the neo-Hookean arterial wall model to fit to it well. It is only when the CA response approaches the inflection point that the model diverges from it. For possible future work, investigation into other hyperelastic material models is recommended so that better fits can be achieved. Material models that have an inflection point or increasing stiffness would benefit the CA and SA models, respectively, with more material parameters allowing control over the response characteristics. Both arteries stiffen significantly after a specific pressure. Collagen fibres are responsible for this behaviour because they begin to be progressively recruited (Holzapfel, Gasser & Ogden, 2000).

The approach and methodology used in this paper has allowed the progressive development of an arterial wall model within commercial software. However, due to time constraints, investigation into material orthotropy, compound cylinders, and solver convergence issues was abandoned. The isotropic assumption of the model limits the value of comparing the SA's pressure-axial responses. Addressing model

assumptions and investigating other hyperelastic material models in further work will likely improve the fit of the pressure-diameter and axial responses. The FEA and analytical validation methodology used provided plausible results. The limitations of it are the final mesh, SDAF convergence, non-linear analysis time control settings, and other inherent FEA limitations. Convergence issues at deformations larger than 20% diametral strain limited the range at which the model could be compared to the CA experimental data.

Conclusion

With a model of an arterial wall being progressively developed within commercial software, while successfully validating with analytical theory and comparing the mechanical responses with experimental data, the paper's aim and objectives have been met. In conclusion:

- The model can simulate the mechanical response of elastic arterial walls for different pressures; however, it can only simulate large deformations of up to approximately 20% diametral strain. This prevented the comparison of the mechanical responses of the rat CA for the full experimental range.

- A convergence method for solving a solution-dependent axial force is presented.

- The mesh independence study showed that the number of elements across the cylinder wall had the greatest effect and that 4 elements was appropriate for this study.

- The neo-Hookean arterial wall model simulated Weizsacker & Pinto's (1988) rat CA well with an RMSE of 0.43 mm Hg for the pressure-diameter response of up to 15% diametral strain.

- It did not simulate Sommer *et al.*'s (2018) SA well as its pressure-diameter response significantly diverged after 2% diametral strain although it had an RMSE of 0.94 mm Hg below this. This suggests that the neo-Hookean material model is not suitable for simulating this subclavian artery.

- The poor fit of the pressure-axial response for the SA shows that material orthotropy should be considered.

- Due to time constraints, material orthotropy, compound cylinders, and convergence issues were not fully investigated.

Recommendations

- Investigation into improving model convergence for diametral strains above 20%. Possible solutions are mesh refinement during solving, optimising boundary conditions for large deformation analysis, and adjusting time control settings.

- Addressing the remaining assumptions of the model. For example, the implementation of orthotropic material properties and multiple layers (compound cylinder). Orthotropic properties could improve the pressure-axial response of the model for the SA.

- Investigation of other hyperelastic material models to achieve more similar behaviour to real arteries, including the consideration of modified hyperelastic models in literature that are for the purpose of arterial wall modelling. Custom material models could be implemented using ANSYS Mechanical APDL.

Acknowledgements

References

Anssari-Benam, A. & Bucchi, A. (2021) 'A generalised neo-Hookean strain energy function for application to the finite deformation of elastomers'. *International Journal of Non-Linear Mechanics*, 128

ANSYS Inc (2011) *ANSYS Mechanical APDL Material Reference*. Release 14.0 edn. Canonsburg, PA:

Boron, W. F. & Boulpaep, E. L. (2017) *Medical physiology*. 3rd edn. Philadelphia, PA: Elsevier.

Burton, A. C. (1954) 'Relation of structure to function of the tissues of the wall of blood vessels'. *Physiological reviews*, 34 (4), pp. 619-642.

Chuong, C. J. & Fung, Y. C. (1984) 'Compressibility and constitutive equation of arterial wall in radial compression experiments'. *Journal of Biomechanics*, 17 (1), pp. 35-40.

Demiray, H. & Vito, R. P. (1991) 'A layered cylindrical shell model for an aorta'. *International Journal of Engineering Science*, 29 (1), pp. 47-54.

Gasser, T. C., Ogden, R. W. & Holzapfel, G. A. (2006) 'Hyperelastic modelling of arterial layers with distributed collagen fibre orientations'. *Journal of the Royal Society Interface*, 3 (6), pp. 15-35.

Hall, J. E. (2015) *Guyton and Hall textbook of medical physiology*. 13th edn. Philadelphia, PA: Elsevier.

Hearn, E. J. (1997a) *Mechanics of Materials 2: The Mechanics of Elastic and Plastic Deformation of Solids and Structural Materials*. 3rd edn. Oxford: Butterworth-Heinemann.

Hearn, E. J. (1997b) *Mechanics of Materials Volume 1 : An Introduction to the Mechanics of Elastic and Plastic Deformation of Solids and Structural Materials*. 3rd edn. Oxford: Butterworth-Heinemann.

Holzapfel, G. A. & Gasser, T. C. (2007) 'Computational stress-deformation analysis of arterial walls including high-pressure response'. *International Journal of Cardiology*, 116 (1), pp. 78-85.

Holzapfel, G. A., Gasser, T. C. & Ogden, R. W. (2000) 'A new constitutive framework for arterial wall mechanics and a comparative study of material models'. *Journal of Elasticity*, 61 (1-3), pp. 1-48.

Holzapfel, G. A., Gasser, T. C. & Stadler, M. (2002) 'A structural model for the viscoelastic behavior of arterial walls: Continuum formulation and finite element analysis'. *European Journal of Mechanics*, A/Solids, 21 (3), pp. 441-463.

Kalita, P. & Schaefer, R. (2008) 'Mechanical models of artery walls'. *Archives of Computational Methods in Engineering*, 15 (1), pp. 1-36.

Kamenskiy, A. V., Dzenis, Y. A., Kazmi, S. A. J., Pemberton, M. A., Pipinos, I. I., Phillips, N. Y., Herber, K., Woodford, T., Bowen, R. E., Lomneth, C. S. & MacTaggart, J. N. (2014) 'Biaxial mechanical properties of the human thoracic and abdominal aorta, common carotid, subclavian, renal and common iliac arteries'. *Biomechanics and Modeling in Mechanobiology*, 13 (6), pp. 1341-1359.

Kanyanta, V. & Ivankovic, A. (2010) 'Mechanical characterisation of polyurethane elastomer for biomedical applications'. *Journal of the Mechanical Behavior of Biomedical Materials*, 3 (1), pp. 51-62.

Kyriakides, S. & Yu-Chung, C. (1991) 'The initiation and propagation of a localized instability in an inflated elastic tube'. *International Journal of Solids and Structures*, 27 (9), pp. 1085-1111.

Marckmann, G. & Verron, E. (2006) 'Comparison of hyperelastic models for rubber-like materials'. *Rubber Chemistry and Technology*, 79 (5), pp. 835-858.

Marieb, E. N. & Hoehn, K. N. (2015) *Human Anatomy & Physiology*, Global Edition. 10th edn. Harlow (UK): Pearson Education Limited.

Mozafari, H., Zhou, C. & Gu, L. (2019) 'Mechanical contribution of vascular smooth muscle cells in the tunica media of artery'. *Nanotechnology Reviews*, 8 (1), pp. 50-60.

Ogden, R. W. (1984) *Non-linear Elastic Deformations*. Chichester, NY: Ellis Horwood Limited.

Patel, D. J. & Fry, D. L. (1969) 'The elastic symmetry of arterial segments in dogs'. *Circulation research*, 24 (1), pp. 1-8.

Patton, K. T. & Thibodeau, G. A. (2010) *Anatomy & physiology.* 7th edn. St. Louis, MO: Mosby Elsevier.

Roark, R. J. (2000) Roark's formulas for stress and strain. eds. Young, W.C., Roark, R.J. and Budynas, R.G., 7th edn. McGraw-Hill.

Sasso, M., Palmieri, G., Chiappini, G. & Amodio, D. (2008) 'Characterization of hyperelastic rubber-like materials by biaxial and uniaxial stretching tests based on optical methods'. *Polymer Testing*, 27 (8), pp. 995-1004.

Sommer, G., Benedikt, C., Niestrawska, J. A., Hohenberger, G., Viertler, C., Regitnig, P., Cohnert, T. U. & Holzapfel, G. A. (2018) 'Mechanical response of human subclavian and iliac arteries to extension, inflation and torsion'. *Acta Biomaterialia*, 75 pp. 235-252.

Tortora, G. J. & Derrickson, B. H. (2009) *Principles of Anatomy and Physiology: Maintenance and Continuity of the Human Body*. 12th edn. vol. 2. Hoboken: John Wiley & Sons.

Treloar, L. R. G. (1944) 'Stress-strain data for vulcanised rubber under various types of deformation'. *Transactions of the Faraday Society*, 40 pp. 59-70.

von Maltzahn, W. W., Besdo, D. & Wiemer, W. (1981) 'Elastic properties of arteries: A nonlinear two-layer cylindrical model'. *Journal of Biomechanics*, 14 (6), pp. 389-397.

Weizsacker, H. W. & Pinto, J. G. (1988) 'Isotropy and anisotropy of the arterial wall'. *Journal of Biomechanics*, 21 (6), pp. 477-487.